

# Chapter 6

## Modeling Hypoxia and Its Ecological Consequences in Chesapeake Bay

Jerry D. Wiggert, Raleigh R. Hood and Christopher W. Brown

**Abstract** The Chesapeake Bay is a valuable recreational, ecological and economic resource that is subject to environmental hazards, such as harmful algal bloom (HAB) and hypoxia, which can degrade the Bay's health and jeopardize the viability of this important natural resource. As a step toward developing the capability to forecast such hazards, a biogeochemical version of the Chesapeake Bay Regional Ocean Modeling System (ChesROMS) has been developed. The model framework encompasses the physical, biogeochemical and bio-optical effects of river borne sediments, atmospheric deposition, nutrient and dissolved organic matter inputs, and benthic interactions throughout the Bay. These influences all contribute to the evolution of dissolved oxygen in the Bay's waters, in particular the consistent annual development of anoxia in the bottom waters of the mid-Bay region. Here, we report on the performance of a newly developed, mechanistic dissolved oxygen formulation that has been incorporated into the ChesROMS model with the motivation to realistically resolve seasonally developing hypoxia/anoxia in the Bay. Insights into various biophysical interactions and biogeochemical processes of the Bay gained from these numerical experiments are considered, and the application of the ChesROMS model fields in short-term ecological forecast applications is discussed.

**Keywords** Hypoxia • Anoxia • Numerical modeling • Ecological forecasting • ROMS • Chesapeake Bay

---

J.D. Wiggert (✉)

Division of Marine Science, School of Ocean Science and Technology,  
University of Southern Mississippi, Stennis Space Center, MS 39529, USA  
e-mail: jerry.wiggert@usm.edu

R.R. Hood

Horn Point Laboratory, University of Maryland Center for Environmental Science,  
Cambridge, MD 21613, USA

C.W. Brown

Center for Satellite Applications and Research, National Oceanic  
and Atmospheric Administration, College Park, MD 20740, USA

## 6.1 Introduction

Chesapeake Bay is the largest estuary in North America and has the highest land-to-water ratio (14:1) of any coastal water body in the world. The Chesapeake Bay watershed spans more than 64,000 square miles, encompasses the District of Columbia and parts of six states, extends northward to Otsego Lake near Cooperstown, NY and westward to the foothills of the Blue Ridge Mountains, and is home to more than 17 million people. Recreationally, the Bay's sport salt-water fishing industry annually yields \$1.34 billion in sales (National\_Marine\_Fisheries\_Service 2011), and swimming and boating are supported by numerous beaches and safe harbors. Ecologically, vast wetlands surround the Bay and its tributaries and offer a haven for a rich diversity of wildlife. Economically, the Bay supports the livelihoods of many commercial fishermen. The commercial seafood industry contributed \$3.39 billion in sales, \$890 million in income, and nearly 34,000 jobs to the local economy in 2009; furthermore, the Bay is the largest producer of blue crabs in the world, with yearly harvests of approximately 24.9 million kilograms (National\_Marine\_Fisheries\_Service 2011). Clearly, maintaining the ecological health of the Bay is a priority for the quality of life and economic vitality of the mid-Atlantic region.

The seasonal variability of the physical environment within the Bay regulates the biogeochemical processes that in turn provide the framework for supporting these substantial fisheries harvests. The magnitude of the Bay's estuarine circulation is primarily set by the seasonality of the Susquehanna outflow, which typically peaks in the spring and tapers off to a late summer minimum. Seasonally varying wind forcing has also been established as an important contributor to the longitudinal circulation, with wintertime northerly winds acting to reinforce the principal estuarine circulation and southerly winds associated with the summertime Bermuda High acting in opposition to this circulation (Goodrich and Blumberg 1991). Along with its influence on the estuarine circulation, the annual cycle of freshwater inflow is a primary control on the seasonal variation in water column stratification, which is of particular biogeochemical relevance due to how this affects air-sea exchange and therefore in water dissolved oxygen concentration. The annually recurring development of severe hypoxia in the bottom waters of the main stem of the Bay is clearly linked to water column stratification that develops in late spring/early summer (Murphy et al. 2011).

Human activities over the last several decades have led to significant degradation of water quality and ecosystem health in the Bay (Kemp et al. 2005). Associated detrimental impacts include nutrient pollution and the negative consequences of eutrophication such as increased turbidity of Bay waters, which inhibits the growth of submerged aquatic vegetation (SAV) (Moore and Wetzel 2000; Moore and Jarvis 2008). Eutrophication has also amplified the annually recurring manifestation of hypoxia in bottom waters of the Bay, an environmental condition that is harmful to

both invertebrates and fish. All of these negative effects are subject to substantial intra-seasonal and interannual variability that arises due to variations in freshwater/nutrient loading and the above-noted physical drivers (Murphy et al. 2011; Hagy et al. 2005). This variability is so large that it has made it difficult to assess whether efforts to restore the Bay are working; that is, detecting a clear trend is problematic given the system's inherent variability. This variability also makes it difficult to predict what the ecological health of the Bay will be in the future on timescales ranging from days to months to years and under the emerging impacts of global climate change (Najjar et al. 2010).

Developing the ability to predict the timing, location, and intensity of low oxygen events will help mitigate their impacts on human and ecosystem health by providing local, state, and federal agencies with early warnings of their arrival. Furthermore, this capability can be used by managers to evaluate the outcome of different scenarios and select the best alternative in order to better preserve the coastal resources and protect human health.

As part of an effort to predict water quality and ecosystem health in Chesapeake Bay, we have developed the Chesapeake Bay Ecological Prediction System (CBEPS), a three-dimensional, coupled estuarine physical–biogeochemical–ecological modeling system that routinely generates and provides nowcasts and short-term (3-day) forecasts of a broad suite of physical, biogeochemical and ecological properties in the Bay (Brown et al. 2013). This modeling system is built upon the Chesapeake Bay Regional Ocean Modeling System (ChesROMS) (Xu et al. 2011), an implementation of the open source Regional Ocean Modeling System (ROMS) (Shchepetkin and McWilliams 2005) for Chesapeake Bay.

The ChesROMS's biogeochemical model was developed to capture the spatio-temporal variability of the Bay's phytoplankton and nutrient distributions. Capturing the annually recurring seasonal onset of hypoxia at depth in the mid-Bay region (Hagy et al. 2004) was another specific objective of the model's development. The focus on hypoxia necessitates the inclusion of an active dissolved oxygen (DO) component in the biogeochemistry. Fulfilling this need represents a challenge in terms of maintaining sufficient complexity to capture the seasonally recurring transition to hypoxic/anoxic waters in a setting where the influence of benthic–pelagic coupling (i.e., exchange of dissolved nutrients and DO) plays a critical role in the overall elemental cycling of the Chesapeake Bay system. In addition, this model must be capable of capturing interannual variability in the Bay's biogeochemical properties and DO. Finally, a streamlined approach is needed for routine application of the ChesROMS biogeochemical model to obtain the nowcasts and short-term forecasts of ecosystem function that inform CBEPS (cf., Brown et al. 2013), and to expeditiously perform longer-term runs (e.g., annual and interannual hindcasts) used for synthesis studies of the Chesapeake Bay system.

In this paper, we describe the ChesROMS biogeochemical model, focusing on the model components that have been developed and implemented to simulate

nutrient cycling under seasonally developing hypoxic and anoxic conditions in both the water column and sediments of Chesapeake Bay. The solutions presented here were all obtained through application of forcing fields from 1999, which was chosen as a focus for the biogeochemical model's development since it represents a typical hydrologic flow regime. The three primary aspects of the Bay's biogeochemical variability we targeted as key features to capture in the model simulations were the phytoplankton bloom dynamics, the spatio-temporal variation of nutrient distributions, and the onset and persistence of severe hypoxia along the main stem. We found that there are inherent tradeoffs to these three modeling objectives, whereby increased skill in one aspect can be countered by a significant degradation of one or both of the other objectives. Here, we report on our success in simultaneously attaining these three objectives, review the new insights into the workings of the Chesapeake Bay system that were gained, and outline future steps for incorporating these insights into ongoing research activities and operational model development efforts.

## 6.2 Methods

### 6.2.1 *ChesROMS: Physical Model and Forcing Fields*

ChesROMS is set up as a three-dimensional, sigma-coordinate model, with a horizontal resolution of 1 to 5 km and 20 vertical levels; this configuration is used to simulate the circulation and physical properties (temperature, salinity, density, velocity and mixing) of the estuary (Fig. 6.1). The physical implementation of the ChesROMS model employed for the results presented here is identical to that reported by Xu et al. (2011). A synopsis of the model setup is presented here; for full details of the implementation, validation and assessment of model skill, the reader is invited to consult the Xu et al. foundational effort.

The ChesROMS physical model provided the capacity to simulate the estuarine circulation in Chesapeake Bay that is principally controlled by hydrologic inputs from nine freshwater sources distributed around the Bay (Xu et al. 2011). The principal sources into the Bay are the Susquehanna (51%), Potomac (18%) and James (14%) Rivers, with further contributions from the Patuxent, Rappahannock and York Rivers and sources on the Eastern Shore (Guo and Valle-Levinson 2007). Forcing of the ChesROMS model consists of lateral boundary conditions associated with the noted river inflows, atmospheric boundary conditions (heat and momentum fluxes) obtained from the NARR reanalysis produced by NCAR, tidal forcing at the Bay's mouth from the ADCIRC EC2001 tidal database along with tide station data from Wachapreague, Virginia and Duck, North Carolina. At the model's open boundary with the North Atlantic, salinity and temperature were nudged to climatological values in the 2001 World Ocean Atlas.

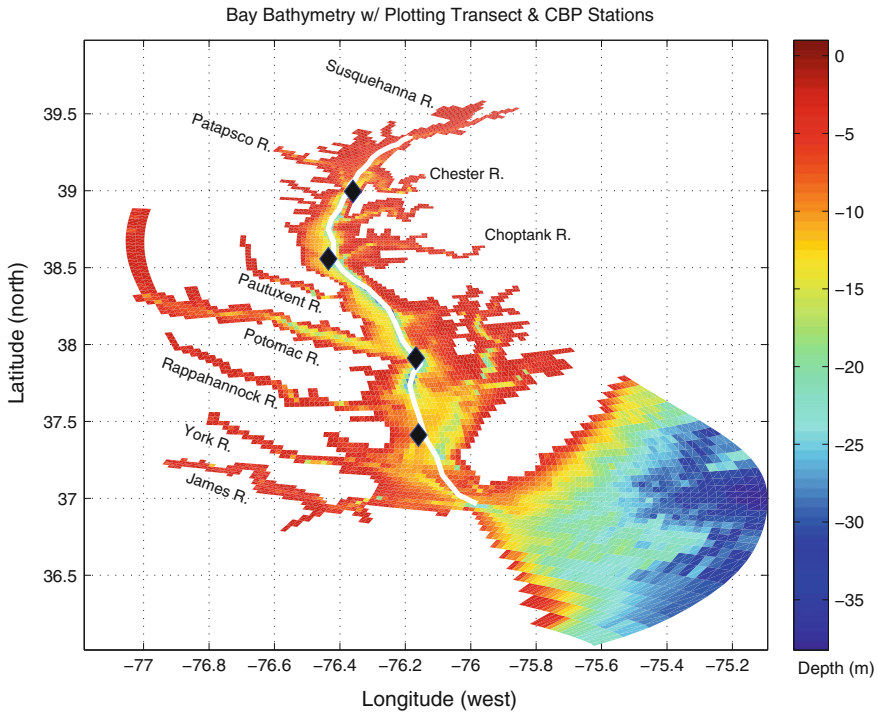


**Fig. 6.1** Bathymetry for the ChesROMS model. The *white line* shows the track of data pulled in making along-bay section plots. The *black diamonds* show the CBP sites that are used in model-data comparisons of upper, mid-, and lower Bay physical and biogeochemical fields. From north to south, the four CBP sites are CB3.3C, CB4.3C, CB5.3 and CB6.3. The principal rivers flowing into Chesapeake Bay are noted

### 6.2.2 ChesROMS: Biogeochemical Model Configuration

A relatively simple NPZD-type ecosystem model has been implemented as a fully coupled component of ChesROMS. The Fennel et al. model (2006) that is provided as a standard component of the ROMS source (<http://www.myroms.org>) forms the basis for the ChesROMS ecosystem model (Fig. 6.2). Here, we describe how the model has been constructed and the capabilities that we have introduced in order to capture the elements of the Bay's biogeochemistry that were not accounted for in the standard ROMS release. Due to space considerations, the detail of the biogeochemical equations that we developed is not included herein. For the reader with interest to pursue these modifications in more depth, a slightly modified version of our biogeochemical formulations has been documented in Feng et al. (2015).

The ChesROMS ecosystem uses nitrogen as its fundamental currency but also includes a simple parameterization of phosphorus limitation. The formulation of an water light model specifically developed for the Bay by Xu et al. (2005) has been

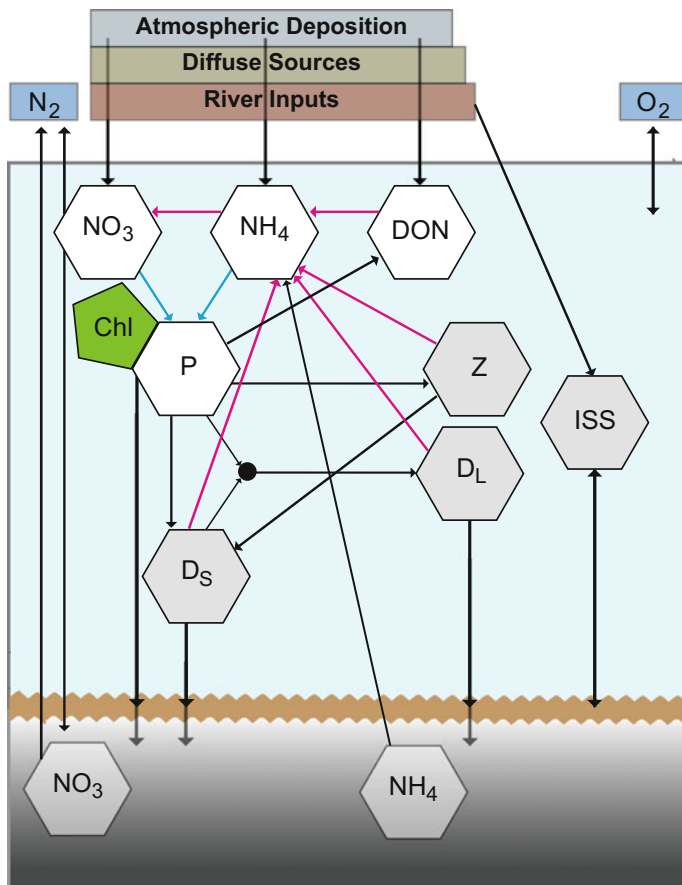


**Fig. 6.2** Diagram for the ChesROMS biogeochemical model, illustrating the flows of nitrogen through the model's state variables. Benthic, terrestrial and atmospheric sources and sinks accounted for by the model are shown. The *gray* backgrounds of Z,  $D_S$ ,  $D_L$  and ISS represent these constituents' role in attenuating downwelling irradiance. Similarly, the *green* background of CHL represents its role in attenuating downwelling irradiance, where CHL is a diagnostic variable of the phytoplankton state variable for which Chl:N varies with environmental conditions (Geider et al. 1997). The *black circle* represents the formation of large detritus ( $D_L$ ) through the aggregation of phytoplankton (P) and small detritus ( $D_S$ ). The *light blue* background of the *upper box* represents the dissolved oxygen within the water column that is subject to atmospheric exchange, variability in stratification and biotic generation and utilization. The *cyan arrows* represent production of oxygen via photosynthesis while the *magenta arrows* in the flow chart represent respiratory processes that take up oxygen. Drawdown of nitrate to fuel benthic denitrification and benthic efflux of ammonium into the water column are indicated by the pathways of  $NO_3$  into and  $NH_4$  out of the benthos

adopted, with model salinity (as a proxy for CDOM (colored dissolved organic matter)) contributing to attenuation of downwelling irradiance, along with chlorophyll and inorganic suspended solids (ISS). The ecosystem tracks phytoplankton

biomass, and organic and inorganic components of nutrient and particulate constituents (Fig. 6.2). The phytoplankton constituent in the model has an associated chlorophyll representation that is based on a Chl:N ratio that is modulated by the light field (Geider et al. 1997). As part of the particulate organic constituents, two detritus size classes are included, where large detritus ( $D_L$ ) is generated through the aggregation of small detritus ( $D_S$ ) and phytoplankton (P) (black circle, Fig. 6.2). A single zooplankton size class with grazing rate modulated by temperature (Huntley and Lopez 1992) contributes to the small detritus pool via sloppy feeding and mortality. A dissolved organic nitrogen (DON) component has been added to accommodate riverine-associated DON loadings that contribute significantly to the Bay's overall nitrogen budget, which exhibits increasing DON:DIN ratio toward the Bay mouth (Bradley et al. 2010). In addition to the flows of nitrogen through the ChesROMS ecosystem noted here, the benthic, terrestrial and atmospheric sources and sinks incorporated in the ecosystem model are represented in the wire diagram (Fig. 6.2).

Dissolved oxygen (DO) concentration is mechanistically determined, with seasonal transitions toward anoxia accomplished by inclusion of explicit water column denitrification based on Oguz (2002). Within the water column, DO-based transitions between nitrifying (normoxic) and denitrifying (hypoxic) conditions are applied that modulate the remineralization of detritus by aerobic and anaerobic bacteria; zooplankton activity and metabolic losses are linked to the nitrification formulation and are thus ramped down where hypoxia is established and as it intensifies. The sources and sinks of DO associated with these biogeochemical processes in the water column are indicated on the wire diagram by the cyan (production) and magenta (uptake) arrows (Fig. 6.2). The benthic biogeochemical model of Fennel et al. (2006) that was developed for normoxic water column applications has been extended by linking benthic exchanges to the dissolved oxygen concentration of overlying bottom waters using a Michaelis–Menten-based formulation.

Through this benthic exchange linkage the model is set to: (1) mechanistically modulate the drawdown of water column DO at depth to fuel benthic denitrification and; (2) capture the observed amplification of ammonium efflux from the benthos and onset of nitrate influx to the benthos as benthic denitrification intensifies (see Fig. 6 in Middelburg et al. 1996). The Michaelis–Menten-style formulation applied to control these benthic exchanges is based on published observations from the Bay that relate ammonium efflux to bottom DO (Rysgaard et al. 1994; Cowan and Boynton 1996). A second Michaelis–Menten style mechanistic link to nitrate concentration in overlying bottom waters is implemented to prevent generation of negative concentrations resulting from nitrate drawdown; this inhibition to nitrate drawdown solely affects the benthic interaction with water column nitrate at depth in the model. That is, anaerobic respiration in the benthos that fuels ammonium efflux is assumed to shift to an alternative electron acceptor source (e.g., sulfate) that is not explicitly modeled. Finally, the sinking velocity of the large detritus pool was reduced by 40% in the bottom layer of the model to allow for advective

redistribution of organic matter by the estuarine circulation and to promote oxygen demand in the water column via resuspension.

Point and diffuse source loadings of  $\text{NO}_3$ , and both organic and inorganic particulates, are based on the rates of river inflow and concentrations of  $\text{NO}_3$ , total organic nitrogen (TON) and total suspended solids (TSS) measured along the Bay's boundaries that were obtained from the Chesapeake Bay Program (CBP) data repository (<http://chesapeakebay.net/>). Atmospheric deposition of  $\text{NO}_3$ ,  $\text{NH}_4$  and DON over the Bay are determined from measured rates of wet atmospherically deposited nitrogen from the NADP's Wye Island Station (<http://nadp.sws.uiuc.edu/>) and constant annual rates of dry deposition (Meyers et al. 2001).

### 6.2.3 *Model Assessment and Validation*

The CBP data holdings are an invaluable resource that have been used here both for setting the initial state of the model and for constructing the biogeochemical boundary conditions associated with point and diffuse sources around the Bay (as noted above). These data were also critical for assessing how effective the biogeochemical model is at capturing the seasonal variability, including vertical structure, over the entire estuary. Measurements of chlorophyll,  $\text{NO}_3$ ,  $\text{NH}_4$ , DO and DON were all routinely extracted and used to directly compare the seasonal variability of profiles at a targeted group of CBP stations (3.3C, 4.3C, 5.3 and 6.3) that are representative of the upper, mid- and lower Bay (Fig. 6.1). The three upper stations are also aligned with the outflows (north to south) of the Patapsco, Choptank and Potomac Rivers, while the Lower Bay site is located south of the Rappahannock River outflow.

The CBP measurements were also used to determine an along-Bay quantification of model skill (Willmott 1981) that provided a temporally integrated view of performance over 27 CBP sites along the Bay's main stem. For the results presented herein, skill values for chlorophyll,  $\text{NO}_3$  and  $\text{NH}_4$  are based on the full annual period while the skill values for DO are based on the summer period (May–August). The temporal and spatial alignment of the model output to the CBP profile data are as follows. The time of the data profiles is aligned to the middle of the UTC hour to associate it with the model time step. Spatially, the model values (20 layers) are interpolated to align with the vertical location of the data. In cases for which the measurement location extends beyond the model profile, the bottommost point in the model profile is used.

As a typical hydrological forcing condition, 1999 was deemed an attractive time frame for conducting the development and testing needed for establishing the biogeochemical model and gaining critical insight into its sensitivities. The results presented here will focus on the baseline model implementation and the insights it reveals regarding seasonal variation of bloom dynamics, nutrient availability and dissolved oxygen in the Bay.



## 6.3 Results

### 6.3.1 Seasonal Variability in the Physical Environment

Examining the seasonal and spatial variability in the Bay’s salinity field reveals the physical setting that controls its biogeochemical processes. The comparison of modeled salinity with co-located measurements drawn from the CBP observations database at the four target stations (3.3C, 4.3C, 5.3 and 6.3) is shown in Fig. 6.3. These point-to-point model-data plots provide a direct comparison of the 15 CBP salinity profiles obtained during 1999 at the four stations highlighted. For this comparison, the smaller symbols at each profile location represent shallower sample depth.

Some generalities that can be drawn from this comparison are that at the two northern sites (3.3c and 4.3c, Fig. 6.3), bottom waters in the model are fresher than the observed condition until the fall when the model is consistent with the data. Surface waters in the model are also consistently fresher at the northernmost station

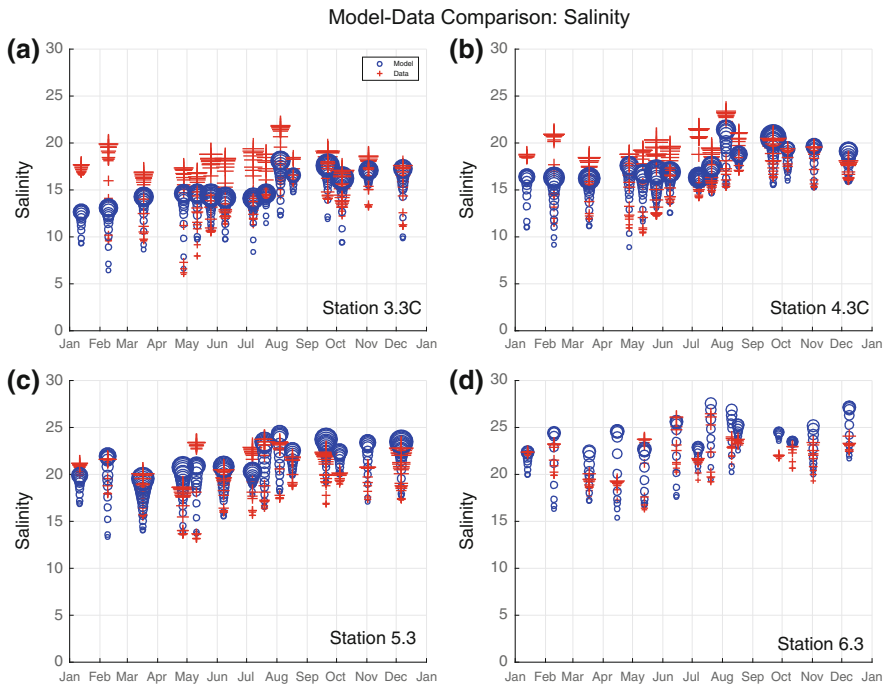


**Fig. 6.3** Observed (+) and modeled (O) salinity in 1999 at four CBP stations: **a** CB3.3C; **b** CB4.3C; **c** CB5.3; and **d** CB6.3 (from upper- to lower Bay). Each vertical group of symbols represents a vertical profile at the corresponding time. Size of the symbols is coded by depth with bigger symbols for greater depth. The along-Bay distribution of these CBP stations is indicated by the *black diamonds* on Fig. 6.1

(3.3c), except during the spring freshet and in November (Fig. 6.3a). At station 4.3c (Fig. 6.3b), the surface waters are slightly fresher than observed through May; over the rest of the year, the model accurately represents surface salinity. Overall at station 5.3 (Fig. 6.3c), the salinity range for each profile over the course of 1999 is well represented by the model. The model does exhibit a tendency toward too salty conditions at depth after July. This tendency (model salinity greater than observed at depth) is more pronounced at station 6.3 (Fig. 6.3d).

Vertical sections of salinity along the Bay's main stem, for April, May, August and October, are shown in Fig. 6.4. The magenta diamonds along the distance axis represent the location of the four CBP stations featured in Fig. 6.3, while the along-Bay distance is in reference to the mouth of the Susquehanna River in Harve de Grace, MD. The extraction path of the along-Bay section from the model results follows the Bay's main stem (Fig. 6.1, white line).

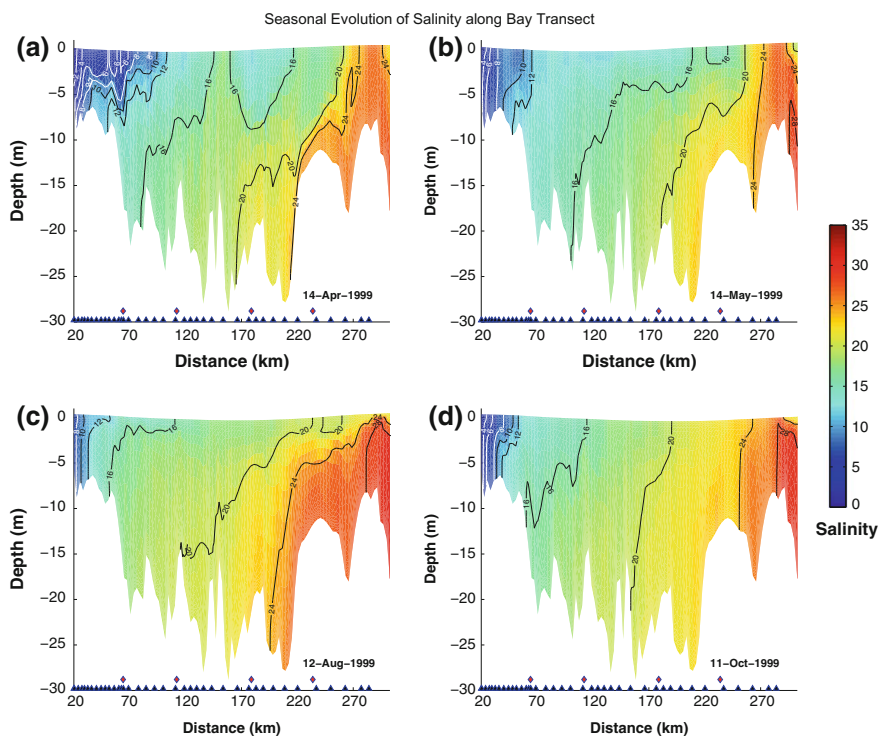


**Fig. 6.4** Along-Bay vertical sections showing the seasonal progression of salinity for: **a** 14 April; **b** 14 May; **c** 12 August; and **d** 11 October. The triangles along the distance axis represent the extraction points used in forming the skill metric (Fig. 6.8). The four *diamonds* (set above the *triangles*) show the four model-data comparison sites (Figs. 6.3, 6.5 and 6.6). The northernmost point of the data extraction track (39.36 °N, 76.19 °W, Fig. 6.1), which is approximately 20 km south of Harve de Grace, MD, serves as the basis for the distance axis

The mid-April time frame of the first salinity section is chosen to align with the seasonal peak in freshwater discharge, which typically occurs late March to early April (Sanford et al. 2001; Schubel and Pritchard 1986). Over the course of the 6 months shown in Fig. 6.4, the freshwater plume associated with the inflow of Susquehanna River water exhibits a clear peak in its extent in the mid-April panel (Fig. 6.4a) with salinities of 12 or less extending ~110 km downstream of the river mouth. The profile from the end of April at station 3.3c (Fig. 6.3a) indicates that surface salinity is accurately captured in the model, whereas the deep values are fresher by ~20%. An interesting feature of the mid-April salinity section is the shoaling of the  $S = 16$  isohaline at 155–165 km and the freshening of surface waters farther downstream, where the  $S = 16$  isohaline again outcrops oceanward of 220 km (Fig. 6.4a). Examining an animation of model salinity sections reveals that this mid-Bay outcropping of the  $S = 16$  isohaline occurs intermittently, and exhibits pronounced variability, from mid-February through mid-June. The fresher waters downstream of this outcrop location, which are bounded by the  $S = 16$  isohaline when the outcrop events occur (Fig. 6.4a), are aligned with the Potomac River inflow. The magenta diamond at ~180 km downstream distance, which demarks CBP station 5.3, is adjacent to the mouth of the Potomac (Fig. 6.1).

The 6-month sequence of salinity sections provides a useful illustration of the evolution of surface salinity in the Bay (Fig. 6.4). The freshwater discharge from the Susquehanna River in May is typically 40–50% lower than the peak discharge of the late March/early April time frame. The retreat of the low salinity feature at the head of the Bay in May (note the  $S = 8$  and  $S = 12$  isohalines) clearly reflects this discharge reduction (Fig. 6.4a, b). The freshening of the mid-Bay region is also apparent, with the  $S = 16$  outcrop no longer present in the mid-Bay (Fig. 6.4b). This results from the progression of the spring freshet down the Bay and the various lateral inputs (e.g., the Potomac and Patuxent Rivers).

The evolution of the estuarine circulation's return flow is represented by the  $S = 16$  and  $S = 20$  isohalines in the 6-month sequence (Fig. 6.4). By May, the bottom expression of both isohalines has shifted toward the Bay mouth coincident with the noted freshwater inflow. Over the summer, the two isohalines propagate 40–50 km northward (Fig. 6.4b, c). Over the summer months, model salinities at depth for the two southern stations show good agreement with the CBP measurements (Fig. 6.3c, d) while the two northern stations are consistently less salty than observed (Fig. 6.3a, b). In the fall this bias shifts, with bottom salinities at the two northern stations represented well in the model while the two southern stations tend toward being too salty. The fall salinity transect reveals the reduction in the strength of the return flow and the onset of fall breakdown of stratification with seasonal cooling (Fig. 6.4d).

As indicated above, the distinction in bottom salinity between the model and the observations at station 3.3c persists through September (Fig. 6.3a); this indicates that the return flow of the estuarine circulation in the model is slightly too weak. For the sections of model salinity, this suggests that the accumulation of elevated salinity waters at the Bay mouth is apparent as the seasonal evolution unfolds is overstated (Fig. 6.4b, c). Thus, deep salinities will tend to be too high near the Bay

mouth and too low in the mid- and upper Bay, as is generally apparent in the model-data comparison time series (Fig. 6.3). This aspect of the simulated physical environment has significant implications for the functioning of the model's biogeochemical constituents, in particular the DO evolution that is attained.

### 6.3.2 *Seasonal Variability of Biochemical Constituents*

Model-data comparison for biochemical constituents of the model (chlorophyll,  $\text{NO}_3$  and  $\text{NH}_4$ ) for the two northern sites, where seasonal anoxia manifests, is shown in Fig. 6.5. The chlorophyll comparison at the northernmost site shows that the range in chlorophyll concentrations is consistent with the measurements (Fig. 6.5a). The spring bloom onset is captured, though the bloom's persistence in the model extends to early May prior to decreasing in late May and into the summer months. The observations indicate that the spring bloom begins to ramp down a couple weeks earlier than in the model; however, the maximum surface chlorophyll concentration ( $>40 \text{ mg m}^{-3}$ ) was measured in late May. During summer, modeled chlorophyll is within the observed range, though the model's subsurface values are consistently higher than the minimum observed concentrations. During fall and early winter, chlorophyll in the model consistently exceeds the measured values over the whole water column. At station 4.3C, the spring bloom in the model also persists longer into the early summer (Fig. 6.5b). Interestingly, during the summer and into the fall the model succeeds in capturing the minimal chlorophyll concentrations at depth that are seen in the data.

The model-data comparison of nitrate provides some insight into the functioning of the model's ecosystem. At both locations, observed nitrate concentrations during late April/early May significantly exceed the modeled values (Fig. 6.5c, d). This suggests that the termination of the spring phytoplankton bloom is due to grazer control, indicating that zooplankton activity in the model does not ramp up as quickly. Minimal values of nitrate over the summer months over the entire water column are accurately represented in the model at station 3.3c, as is the subsequent enrichment in the fall/early winter period (Fig. 6.5c). At station 4.3c, the very low summertime nitrate values are also captured; however, concentrations in the latter months are 2–3 times greater than observed (Fig. 6.5d). The model does accurately capture the observed high bottom-water nitrate concentrations.

The ammonium comparison shows that the model does a good job of simulating low surface concentrations over almost the entire seasonal cycle (Fig. 6.5e, f). Departures from the measured low surface ammonium values ( $<0.6 \mu\text{M}$ ) in the model tend to occur in late summer (particularly mid-August) and in the early winter in the mid- to upper Bay (Fig. 6.5e, f) as well as the lower Bay (not shown). Examining animations of along-Bay sections of ammonium indicate that when they appear, these instances of elevated surface ammonium concentrations in the model result from vertical mixing that homogenizes the water column distribution (data not shown). As this mechanism implies, maximum ammonium concentrations

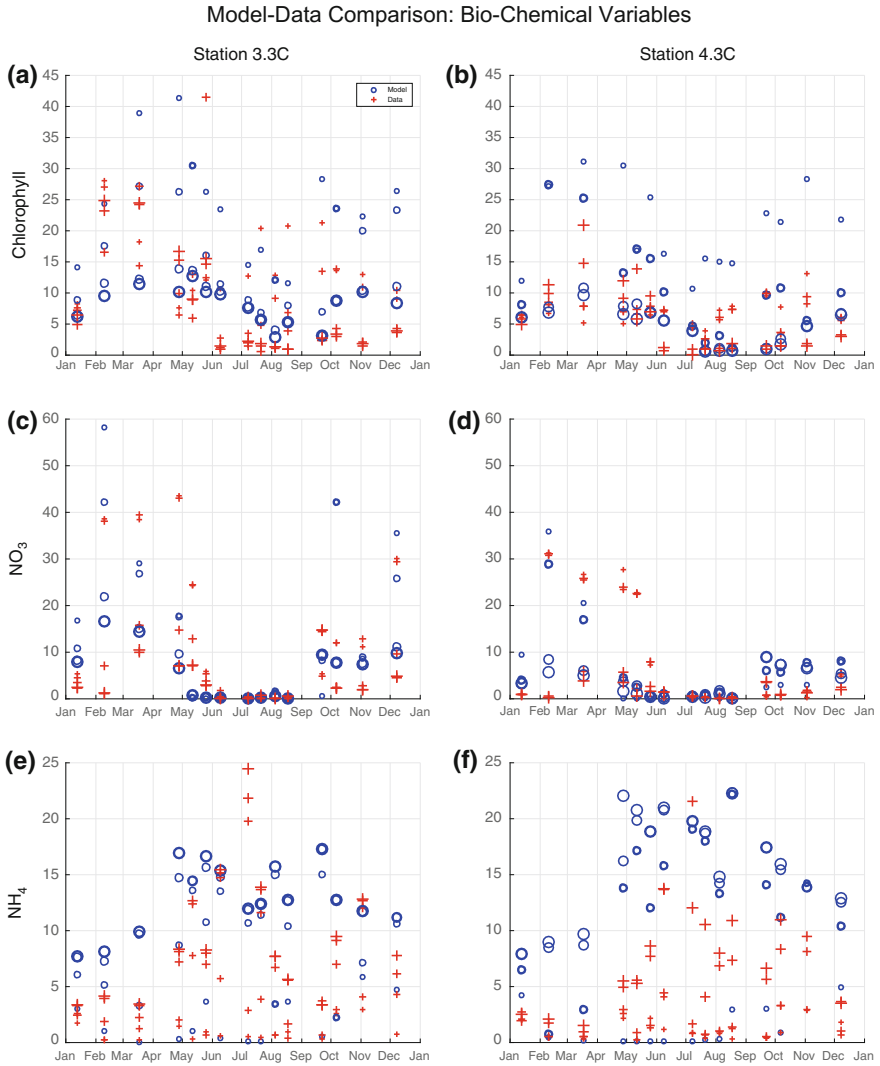


**Fig. 6.5** Observed (+) and modeled (O) comparison of biochemical variables at two CBP stations from the upper (3.3C) and mid-Bay (4.3C): **a, b** chlorophyll (mg m<sup>-3</sup>); **c, d** nitrate (μM); and **e, f** ammonium (μM). Each vertical group of symbols represents a vertical profile at the corresponding time. Size of the symbols is coded by depth with bigger symbols for greater depth. The along-Bay distribution of these CBP stations is indicated by the *black diamonds* on Fig. 6.1

occur in bottom waters that are in contact with the benthos. Peak ammonium values at depth in the model occur consistently throughout the seasonal cycle; the observed vertical distributions also follow this pattern (Fig. 6.5e, f). While the simulation's peak bottom concentration values are consistent with the highest observed values,

modeled concentrations in the lower half of the water column are for the most part higher than observed and these elevated values at depth are clearly more persistent.

### 6.3.3 Dissolved Oxygen (DO) Results

The dissolved oxygen comparison shows that the model captures the general features of the seasonal cycle for the upper, mid and lower regions of the Bay, with peak concentrations in the spring, decreasing concentrations from late spring through the summer and re-oxygenation of the water column initiating in the fall (Fig. 6.6). A more complete representation of this seasonal evolution of dissolved oxygen in the model is revealed in the along-Bay sections (Fig. 6.7). Fully oxygenated springtime surface waters are clearly represented in the section plots; this DO condition can be seen to extend over the entire Bay (Fig. 6.7a). The late spring distribution shows reduction of dissolved oxygen concentrations over the whole water column and the

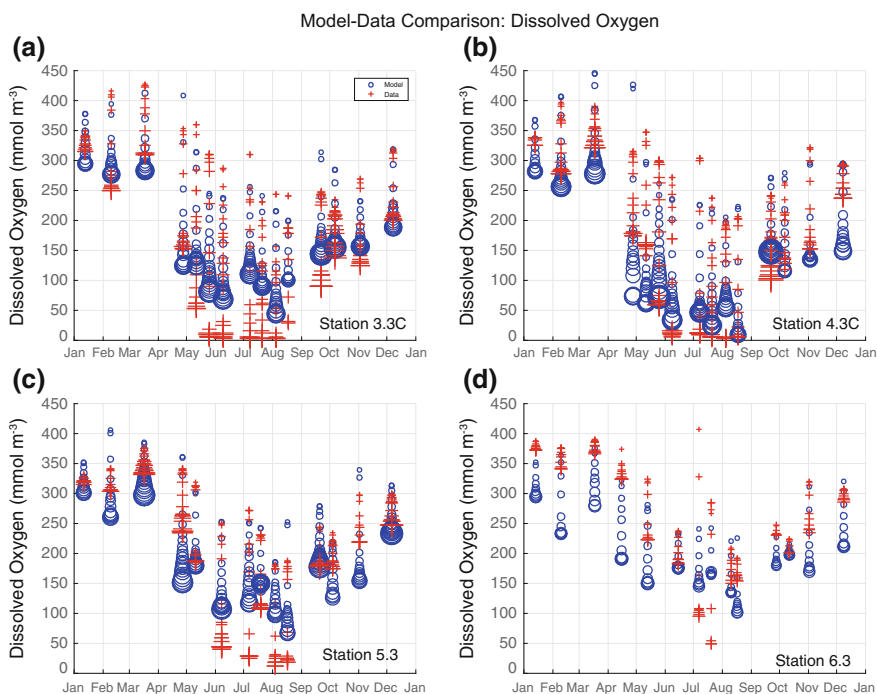


**Fig. 6.6** Observed (+) and modeled (O) dissolved oxygen ( $\text{mmol m}^{-3}$ ) in 1999 at four CBP stations: **a** CB3.3C; **b** CB4.3C; **c** CB5.3; and **d** CB6.3 (from upper- to lower Bay). Each vertical group of symbols represents a vertical profile at the corresponding time. Size of the symbols is coded by depth with bigger symbols for greater depth. The along-Bay distribution of these CBP stations is indicated by the *black diamonds* on Fig. 6.1

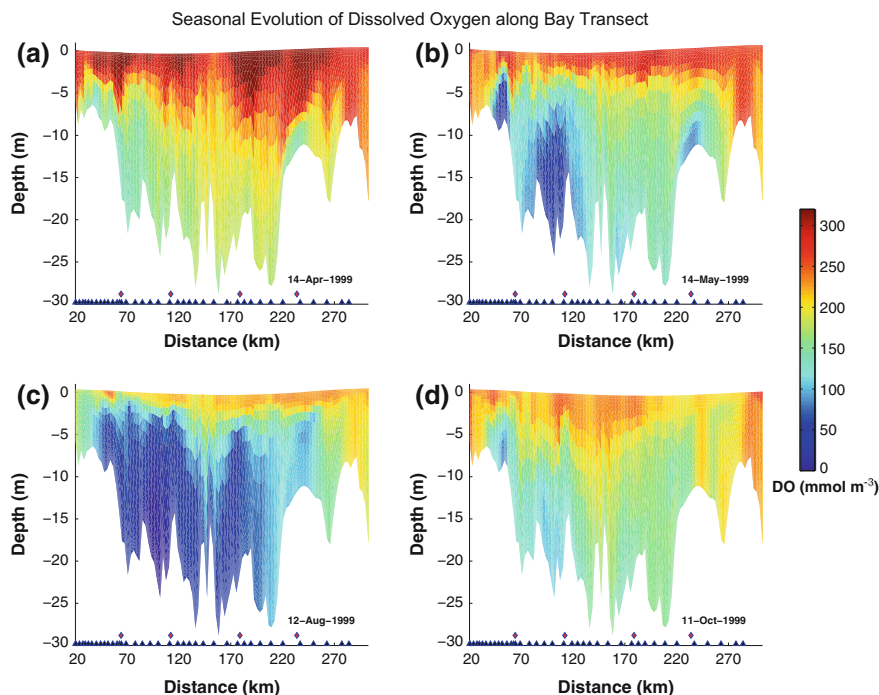


**Fig. 6.7** Along-Bay vertical sections showing the seasonal progression of dissolved oxygen ( $\text{mmol m}^{-3}$ ) for: **a** 14 April; **b** 14 May; **c** 12 August; and **d** 11 October. The triangles along the distance axis represent the extraction points used in forming the skill metric (Fig. 6.8). The four diamonds (set above the triangles) show the four model-data comparison sites (Figs. 6.3, 6.5 and 6.6). The northernmost point of the data extraction track ( $39.36^\circ\text{N}$ ,  $76.19^\circ\text{W}$ , Fig. 6.1), which is approximately 20 km south of Harve de Grace, MD, serves as the basis for the distance axis

appearance of very low bottom-water concentrations at several locations (Fig. 6.7b). These low DO hotspots in the late spring distribution are most pronounced in the mid- to upper Bay with two distinct features that appear just above the two northern CBP focus stations (3.3C, 4.3C); thus, they are situated just upstream of the inflows of the Patapsco and Choptank rivers. The model-data comparison for these two stations shows that the model captures the timing of this hypoxia onset in late spring quite well (Figs. 6.6a, b and 6.7b). In addition, moderate DO concentrations at this time ( $\sim 180 \text{ mmol m}^{-3}$ ) are very accurately represented at station 5.3 (Fig. 6.6c). At station 6.3, the model consistently overestimates DO drawdown at depth through the late spring (mid-May) time frame (Fig. 6.6d).

The establishment of persistent summertime hypoxia is achieved at station 4.3C and intermittently realized at stations 3.3C and 5.3 (Fig. 6.6a–c). All three of these sites exhibit hypoxic conditions in the summer, with the two northern locations reaching full anoxia beginning in late May to early June that persists through the end of August (Fig. 6.6b, c). In the results shown here, full anoxia in the model's

bottom waters is only achieved at station 4.3C in mid-July to mid-August (Fig. 6.6b). However, several other of the CBP station locations in this mid-Bay region also achieve summertime anoxia in the bottom DO concentrations in the model (4.1C, 4.3 W, 5.2, not shown). Further, daily maps of modeled bottom DO over the Chesapeake Bay domain reveals that hypoxic to anoxic conditions extending from the Potomac River inflow (station 5.3) to just north of the Patapsco River inflow (station 3.3C) occur intermittently in late June through July and more persistently throughout August (not shown). The along-Bay section for mid-August illustrates this extensive latitudinal range of very low DO conditions and indicates that hypoxia can range over 15 meters of the water column and extend to within 5 meters of the surface (Fig. 6.7c).

The timing of onset of re-oxygenation of the water column in mid-September for the upper and mid-Bay stations is nicely captured by the model (Fig. 6.6a–c). Further the ongoing evolution of re-oxygenation through early December is well represented. Except for waters proximal to the Patapsco outflow (Fig. 6.7d), the along-Bay section for mid-October indicates that the entire estuary has returned to oxic condition. The CBP data support the model's indication that the main stem region near the Patapsco outflow is a low DO hotspot in the late fall/early winter time frame, as it is the only site where DO is below  $150 \text{ mmol m}^{-3}$  in November and below  $200 \text{ mmol m}^{-3}$  in December (Figs. 6.6 and 6.7d).

### ***6.3.4 Assessment of Model Skill and Parameter Sensitivities***

With the goals of attaining fidelity in the model's representation of phytoplankton bloom dynamics, spatio-temporal variation of nutrient distributions and the onset/persistence of severe hypoxia in the mid- to upper Bay region, an extensive exploration of the ecosystem model's parameter space has been performed. The model-data comparisons of the biochemical fields (e.g., as featured in Figs. 6.5 and 6.6) were a prime component of the solution assessments. The other primary component of these assessments was determination of model skill (as defined in Willmott 1981), which provided an objective, overview characterization of the key state variables for each solution. An aggregate model skill over the 1999 seasonal cycle was calculated using all profile data gathered at each of 27 CBP stations and is presented as an along-Bay variation. The 27 CBP stations chosen for these along-Bay skill assessments range from station CB1.1 ( $39.55^\circ\text{N}$ ,  $76.08^\circ\text{W}$ ) down to CB7.3 ( $37.12^\circ\text{N}$ ,  $76.13^\circ\text{W}$ ); the linear distance of these stations from Harve de Grace, MD is represented by the black triangles on the abscissa of Figs. 6.4 and 6.7. For the most part, these stations lie along the Bay's main stem; however, several sites in the shallower waters adjacent to the main stem are included to provide full representation.

The along-Bay skill within a set of six model solutions for four model state variables (chlorophyll, ammonium, nitrate and dissolved oxygen) is shown in Fig. 6.8. The sidebar of Fig. 6.8 lists the identifiers of the 27 CBP sites included in



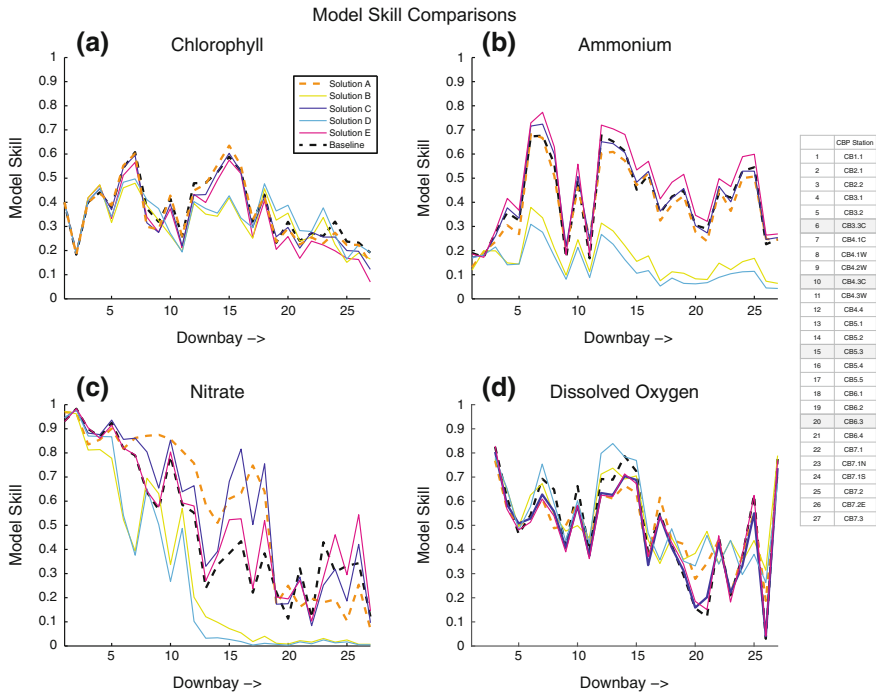


**Fig. 6.8** Along-Bay skill within a set of six model solutions for four model state variables: **a** chlorophyll, **b** ammonium, **c** nitrate and **d** dissolved oxygen. An aggregate of along-Bay skill assessments is determined for 27 CBP stations that range from station CB1.1 (39.55 °N, 76.08 °W) down to CB7.3 (37.12 °N, 76.13 °W). The model-data pairs contained within each aggregate include all depths for every profile obtained by the CBP sampling in 1999 for the chlorophyll, ammonium and nitrate skill plots. For the dissolved oxygen skill plot, the May–August time frame was targeted to gain clearer insight into model performance during the summer hypoxia regime. The complete list of station IDs from which data are drawn for the skill determination is given in the included table

the skill determinations, with an integer index noting their ordering in the down Bay direction. The four CBP stations featured in the model-data comparisons (black diamonds, Fig. 6.1) are indicated by gray shading in this site listing. While skill in the model state variables throughout the Bay was desired, the skill values for DO at sites 6–7 and 12–15 were a focal point for assessing how well summertime hypoxia onset and persistence were attained. These two along-Bay foci, respectively, coincide with the Patapsco/Chester River and Potomac River inflows (Fig. 6.1). It should be noted that differences in DO skill achieved at these sites were closely examined since even minor improvement in skill at these locations was indicative of significant improvement in the summertime evolution of bottom DO concentration in the model, in particular with regard to transitioning to and maintaining hypoxic conditions.

The six featured model solutions are chosen to illustrate the tradeoffs in the fidelity of these biochemical fields that are commonly realized; that is, improvements in one of the targeted system attributes achieved through parameter adjustment are typically accompanied by some degree of degradation in one (or both) of the other attribute targets. The skill assessments shown in Fig. 6.8 represent a progression of overall improvement in model skill as parameter adjustments are adopted, albeit with tradeoffs as detailed below. In previous sensitivity analyses leading up to the group of solutions shown in Fig. 6.8, a diverse range of the model's ecosystem functionalities were explored that assessed maximum nitrification rate, temperature dependence of phytoplankton growth rate and zooplankton grazing rate, and the aggregation parameter that modulates formation of large detritus (represented by the black circle in Fig. 6.2). As a result of this sequence of parameter explorations, model solution A was achieved (dashed orange line, Fig. 6.8).

A particular target outcome that motivated the parameter exploration reported here was to improve the persistence of summertime mid-Bay hypoxia, which was difficult to achieve. Indeed, the summer evolution of mid-Bay hypoxia in Solution A nicely captures onset in late May/early June but does not maintain the severe hypoxia seen in the observations and actually transitions to non-hypoxic DO concentrations by early August (i.e.,  $>62.5 \text{ mmol m}^{-3}$ , Fig. 6.9a). The five subsequent solutions featured in Fig. 6.8 represent a further parameter exploration that targeted refining the formation, water column processing, and benthic delivery of organic matter in the model with the aim of improving persistence of hypoxia during the stratified, summer season. The skill curves for the baseline solution are for the standard run from which all of the model-data shown herein are taken (Figs. 6.3, 6.4, 6.5, 6.6 and 6.7). The skill curves for solutions B–E in Fig. 6.8 highlight intermediate stages from solution A (orange dashed line) that led to the baseline run (black dashed line). Table 6.1 provides a synopsis of the model parameters used for each skill assessment, how the values were adjusted and their impact on the ecosystem.

In the original water column denitrification formulation that we adopted from Oguz (2002), symmetric ramps for switching on/off nitrification and denitrification as conditions transitioned from normoxic to anoxic were employed. For solution B (Fig. 6.8, olive solid line), an asymmetry was introduced via modification of the half-saturation coefficient for the denitrification curve (KDNF, Table 6.1). This asymmetry acted to slightly retard the net remineralization by aerobic and anaerobic bacteria of both detrital size classes, thus resulting in slight amplifications of oxygen uptake within the water column and delivery of organic matter to the benthos. Relative to solution A, solution B exhibited a clear improvement in DO skill at upper and mid-Bay sites (6–7, 12–15), a mixed influence on chlorophyll and a significant degradation of ammonium and nitrate, particularly in the mid- to lower Bay (Fig. 6.8). The degradation of these DIN forms manifests as concentrations that were in excess of 6 times too high in July/August (ammonium) and October/November (nitrate) (not shown). Excessive ammonium efflux is the underlying cause, with the efflux rate being amplified by both the increased organic

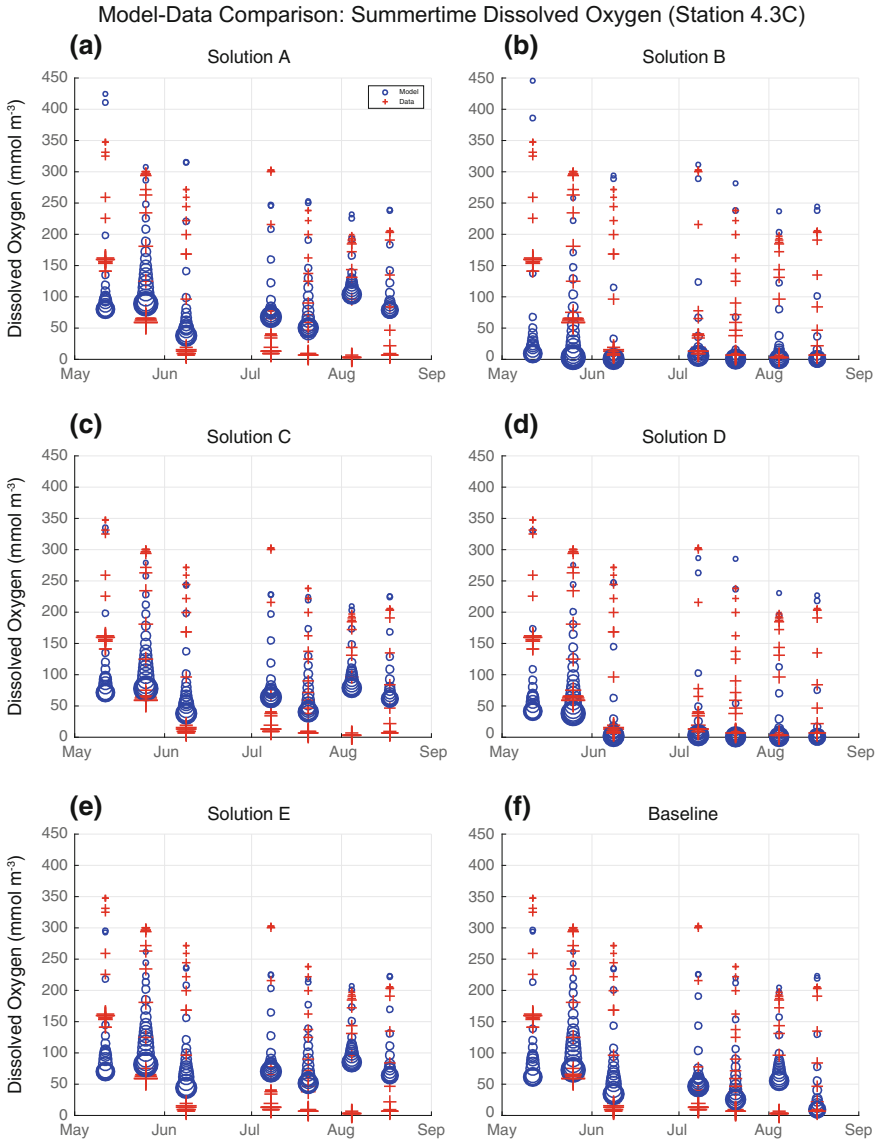


**Fig. 6.9** Observed (+) and modeled (O) dissolved oxygen ( $\text{mmol m}^{-3}$ ) for May–August 1999 at CBP station 4.3C for **a** Solution A, **b** Solution B, **c** Solution C, **d** Solution D, **e** Solution E and **f** Baseline solution. Each vertical group of symbols represents a vertical profile at the corresponding time. Size of the symbols is coded by depth with bigger symbols for greater depth

matter delivery to the benthos and, to a lesser degree, the lower bottom-water DO concentration. These low DO concentrations are clearly apparent in the model-data comparison (Fig. 6.9b). These show that DO values that interact with the benthos,

and modulate benthic exchange rates, successfully capture the summertime persistence of bottom-water anoxia but DO values at mid-depths are lower than observed.

For solution C (Fig. 6.8, blue solid line), the reduction of large detritus sinking velocity in the bottom layers of the model has been relaxed (FwR, Table 6.1) to promote benthic delivery and relieve POM retention in the bottom model layers that amplifies oxygen demand via remineralization in the water column. As intended, this parameter modification returns the mid- to lower Bay DIN fields to a realistic state in the summer to fall time period. However, the summertime onset and evolution of mid-Bay hypoxia is severely degraded, with persistence of bottom anoxia again being poorly captured though with improvement relative to solution A (Fig. 6.9a, c).

For solution D (Fig. 6.8, cyan solid line), a more pronounced asymmetry in the nitrification/denitrification ramps is adopted with the aim of shifting the model into a solution space that can achieve the desired summertime hypoxia behavior (KDNF, Table 6.1). Similar to the solution A -> solution B impact described above, solution D (relative to solution C) exhibits significant degradation of DIN fields in the mid- to lower Bay that is again associated with too high concentrations of ammonium and nitrate in the mid-summer to fall time frame. Also similar to

**Table 6.1** Summary of model parameter adjustments. Column 1 shows the line type, to reinforce the legend on Fig. 6.8. Column 2 gives the run identifier. Columns 3–5 give the details of the affected parameter including its variable name, units, and how its value was modified for the given model run. A summary of the parameter’s direct impact on the model for the given experiment is given in Column 6. Over the progression from solution A to the new baseline solution, the parameter changes are cumulative

Line type	Run ID	Modified parameter	Units	Value adjustment	Modification summary
— — — — —	Solution A				Original solution
—————	Solution B	KDNF	mmol O <sub>2</sub> m <sup>-3</sup>	3.0 -> 2.86	Reduce 1/2 saturation coefficient of denitrification onset curve (KDNF)
—————	Solution C	FwR	N/A	0.9 -> 0.4	Increase D <sub>L</sub> sinking velocity in bottom model layer. wLDet_bottom = (1 - FwR) * wLDet
—————	Solution D	KDNF	mmol O <sub>2</sub> m <sup>-3</sup>	2.86 -> 2.82	Reduce 1/2 saturation coefficient of denitrification onset curve (KDNF)
—————	Solution E	wLDet	m d <sup>-1</sup>	0.5 -> 0.95	Increase D <sub>L</sub> sinking velocity throughout water column
— — — — —	Baseline	KBO2	mmol O <sub>2</sub> m <sup>-3</sup>	26.5 -> 20.0	Reduce 1/2 saturation coefficient applied for benthic biogeochemical exchanges

solution B, the mid-Bay DO fields better capture the onset and evolution of hypoxia in bottom waters, in particular the persistence of anoxia in bottom waters (Fig. 6.9d). However, similar to solution B, mid-depth DO is too low, particularly late July to August time frame (Fig. 6.9b, d). Solution D also realizes the highest skill in chlorophyll in the lower Bay (sites 18–23), which contrasts the poorest skill relative to the other solutions (along with solution B) at mid-Bay sites (13–17).

For solution E (Fig. 6.8, magenta solid line), the sinking velocity of large detritus was increased from 0.5 to 0.95 m/d (wLDet, Table 6.1). This parameter modification promotes flux of organic matter to the benthos and reduces particulate matter loading in the water column, with concomitant impacts on oxygen demand and denitrification. Both DIN fields are positively impacted. Solution E achieves the highest skill in ammonium throughout the Bay and the highest skill in nitrate in the lower Bay. Two pronounced tradeoffs are incurred. The first is the poorest chlorophyll skill in the lower Bay, which results from poorer fidelity of bloom dynamics during the mid-summer to early fall time frame. The second tradeoff is that bottom DO concentrations during summertime are just on the threshold of hypoxic, rather than the severe hypoxia to anoxia that is observed for the June through August time frame (Fig. 6.9e).

For the baseline solution (Fig. 6.8, black dashed line), the half-saturation coefficient in the formulation that links benthic exchanges to the DO concentration of overlying bottom waters is lowered by ~25% (KBO2, Table 6.1). In oxic to marginally hypoxic bottom waters, this modification reduces nitrate drawdown and ammonium efflux, and enhances dissolved oxygen drawdown. The reduced nitrate drawdown has an interesting, though subtle, impact that can be seen when comparing model fields for the mid-Bay stations of the standard run (Fig. 6.5b, d, and f) with those of solution E (not shown). Higher nitrate concentration in late April promotes higher plankton biomass (both P and Z) that leads to higher POM accumulation, relative to solution E, with an associated increase in water column recycling and DO uptake. This combines with the amplified benthic DO drawdown linked with export fluxes to improve hypoxic onset and persistence in the model's bottom waters during the summer (Fig. 6.9e, f).

The summertime DO time series for the six experiments demonstrate the significant variation in the modeled hypoxia evolution at one station (4.3C, Fig. 6.9). Aside from solution B, there is a consistent pattern to hypoxia onset in May. In contrast, the persistence of anoxia in bottom DO and evolution of DO concentration over the water column exhibits a range of responses across the six solutions (Fig. 6.9); this diverse model DO response to the applied parameter modifications is apparent all along the Bay in the skill values (Fig. 6.8d). At station 4.3C, the baseline solution can be seen to provide the best balance between attaining persistent hypoxic bottom DO conditions while maintaining low (non-hypoxic) conditions at mid-depths of the water column (Fig. 6.9). For additional overall comparative perspective for the six solutions in the skill assessments, mean skill values and rankings of the experiments for all four state variables have been collected in Table 6.2. The gray shading applied to some of the cells indicate results where the along-Bay skill is below one standard deviation from the mean for all

**Table 6.2** Summary of impact on model skill as a result of the parameter adjustments (Table 6.1). Column 1 gives the run identifies. Columns 2–5 give the mean along-Bay skill. The temporal range for the mean skill values of chlorophyll,  $\text{NH}_4$  and  $\text{NO}_3$  is annual while for DO it is the summer period (May–August). The rank order over the six solutions in this comparison is given along with the mean skill. The mean and standard deviation for the four parameter skills are given in the two bottom rows. For table cells with italics, the mean along-Bay skill for a given solution is more than one  $\sigma$  below the mean over the six solutions

Run ID	Mean Along-Bay Skill			
	Chl	$\text{NH}_4$	$\text{NO}_3$	DO
Solution A	<i>0.33/5</i>	0.40/4	0.55/2	0.50/3
Solution B	<i>0.32/6</i>	<i>0.17/5</i>	<i>0.26/5</i>	0.53/2
Solution C	0.36/3	0.43/2	0.56/1	<i>0.48/6</i>
Solution D	0.34/4	<i>0.14/6</i>	<i>0.25/6</i>	0.54/1
Solution E	0.37/2	0.48/1	0.52/3	<i>0.49/5</i>
Baseline	0.38/1	0.43/2	0.49/4	0.50/3

experiments. This view of the results, along with the skill and summer DO comparisons (Figs. 6.8 and 6.9), summarizes the tradeoffs in the model’s skill at capturing the observed spatial and temporal variability of the key biogeochemical parameters targeted in this assessment. It is apparent that each solution tended to have an attribute for which it particularly excelled, yet each was also consistently plagued by one (or more) attribute(s) for which performance was particularly poor (e.g.,  $\text{NH}_4$  and  $\text{NO}_3$  skill in solutions B and D, Fig. 6.8b, c). Overall, it can be seen that the baseline solution achieved the best collective fidelity over the spectrum of model attribute objectives articulated in the introduction.

## 6.4 ChesROMS Application to Ecological Forecasting of Chesapeake Bay

The ultimate goal motivating our development of the ChesROMS biogeochemical model is its application as a means of illuminating biogeochemical processes within the Bay (described above) and providing nowcasts and short-term forecasts that can be used to inform the Chesapeake Bay Ecological Prediction System (CBEPS). The CBEPS was created with and for state and federal agencies responsible for monitoring and responding to potentially harmful biotic events and conditions in Chesapeake Bay, such as harmful algal blooms and hypoxia, to forecast these events and aid in mitigating their deleterious effects on human and ecosystem health (Brown et al. 2013).

In the application of CBEPS, the physical and biogeochemical variables are forecast mechanistically using ChesROMS, while the species predictions are generated using a novel mechanistic—empirical approach, whereby real-time output from the coupled physical—biogeochemical model drives multivariate empirical

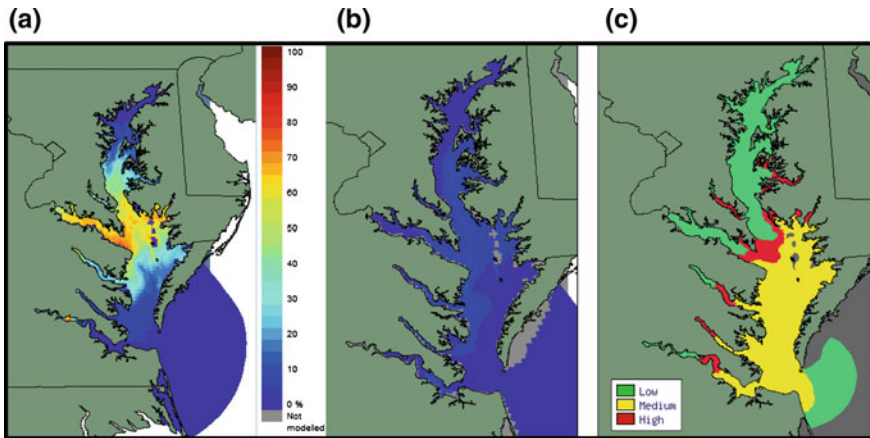


**Fig. 6.10** Examples of species forecasts generated by the Chesapeake Bay Ecological Prediction System (CBEPS). **a** Probability of encountering Atlantic sea nettles, *Chrysaora quinquecirrha*, on 17 August 2007; **b** probability of encountering the pathogenic bacterium *Vibrio vulnificus* on 20 April 2011; and **c** relative abundance of the potentially toxic dinoflagellate *Karlodinium veneficum* on 20 April 2005. Legend: low: 0–10, med: 11–2000 cells/ml, high: >2000 cells/ml. Color bar for likelihood is the same for both A and B. Reproduced with permission from Brown et al. (2013)

habitat suitability models of the target species (see Fig. 3 in Brown et al. 2013). Environmental variables such as water temperature, water clarity, the concentrations of chlorophyll and nutrients, and the probability of encountering or (relative) abundance of several noxious species, such as the Atlantic sea nettle (*Chrysaora quinquecirrha*), a stinging jellyfish, the pathogenic bacterium *Vibrio vulnificus*, and the harmful algal species *Karlodinium veneficum* in the Bay and its tributaries are provided as forecast guidance (Fig. 6.10). Near real-time forecasts of sea nettle distribution have been widely viewed by recreational users, while predictions of *V. vulnificus* appearance are under review by state officials to assist in monitoring recreational exposure (J. Jacobs, pers. comm.) and have been deemed helpful to managers who must decide when to close beaches and shellfish beds (Pace et al. 2015). Hindcasts can be used to explore likely changes in the distribution of these organisms that might occur in the future in response to climate change (Decker et al. 2007; Jacobs et al. 2014).

The capability to predict DO and consequently hypoxic events provides these agencies with a tool that can be used to alert them of these and related potentially harmful conditions. For example, predicting the three-dimensional fields of DO and water temperature can be used by fisheries scientists to assess the volume of suitable habitat for various commercially important fish in the Bay, such as striped bass, and the stress imposed on them by hypoxia and elevated temperatures (Ludsin et al. 2009; Costantini et al. 2008). The hypoxia predictions can also be used tactically by monitoring agencies to strategically design and implement their sampling efforts in Chesapeake Bay and its tributaries. Forecasts are needed more

than ever to guide sampling activities in the field and increase the efficiency of monitoring programs during periods of limited resources. On a longer time horizon, CBEPS/ChesROMS could be extended, given appropriate forcing, to project how anthropogenic effects might impact the timing, distribution, and intensity of hypoxia in the Bay in the future.

In order for the environmental predictions to be useful to the agencies and public, they must be sufficiently accurate with a known degree of uncertainty, reliably available and accessible in a timely fashion, and interpretable by these agencies and its users. CBEPS is located, maintained and run by an academic institution (University of Maryland's Center for Environmental Science at Horn Point Laboratory in Cambridge, MD) that is not funded to offer this degree of service. As a consequence, over the course of CBEPS's lifetime, its predictions have sporadically been unavailable due to problematic issues such as maintaining software licensing, hardware viability and supporting cyberinfrastructure. It does, however, offer a valuable experimental platform to test and assess new ecological forecasting algorithms and models for the Bay and to demonstrate the use of these predictions. Once validated and deemed useful by the community, the newly developed techniques and models can and should be migrated into a true operational environment within an appropriate agency, such as NOAA. This effort is one of several crucial steps in laying the foundation for generating truly operational ecological forecasts in Chesapeake Bay and serves as a roadmap for other locations.

## 6.5 Discussion and Conclusions

The ChesROMS physical model has considerable skill in simulating temperature and, to a lesser degree, salinity in Chesapeake Bay; hindcasts over a 15-year period (1991–2005) reveal that both temperature and salinity fields match well with observations with a correlation of approximately 0.99 and RMSE of 1–1.5 °C for temperature and a correlation of 0.95 and RMSE of 2–2.5 for salinity (Xu et al. 2011). The results presented herein reflect this lower salinity correlation, with bottom waters that are too fresh at the northern sites during summer (Fig. 6.3a, b) and too saline at the southern sites during fall (Fig. 6.3c, d). This model tendency is further demonstrated in the seasonal sections of salinity that reveal an accumulation of high salinity waters near the southern end of the Bay, which should propagate farther up the estuary. This is indicative of an estuarine circulation with a too weak return flow in the model; the core shortcoming leading to this result is an overly smoothed bathymetry with an inadequately resolved deep channel. Higher resolution ROMS simulations have been demonstrated to better resolve the estuarine return flow and more realistically capture along-Bay salinity variability (M. Scully, personal communication). However, the computational demand of such higher resolution configurations makes them impractical to use in most research efforts.

The ecosystem model results from the main solution (Figs. 6.5, 6.6, 6.7 and 6.9) indicate that rather than being solely prescribed by dynamical processes, these fields



are subject, over location and season, to varying blends of physical and biochemical control; this assertion is consistent with that articulated in the synthesis of Kemp et al. (2009). The link between stratification and hypoxia in coastal and estuarine systems is well-documented (Rabalais et al. 2010) and has a clear association in the salinity and DO fields of the model (Figs. 6.3 and 6.6). Contrasting how salinity stratification relates to DO evolution in bottom waters at stations 3.3C and 4.3C underscores the importance of realistically representing stratification of bottom waters, which harkens back to the issues noted above regarding the shortcomings in the estuarine circulation. Comparing the fidelity of bottom salinity at station 3.3C to that at 4.3C in the model (Fig. 6.3a, b), it can be seen that the modeled salinity during the May–August period is notably worse at the more northern site (i.e., where the estuarine circulation is more poorly represented). It is also apparent that the greater skill at capturing summertime onset and persistence of hypoxia at these two sites aligns with how well stratification of bottom salinity is represented (Figs. 6.3a, b and 6.6a, b). Overall, examining these two sites reveals a direct linkage between the degree of mismatch in modeled bottom salinity and how well the temporal evolution of bottom hypoxia is represented.

In contrast, the spring bloom in the model is an example of a biophysical interaction subject to biochemical control where its onset is consistent with the observed timing yet its persistence is longer than is apparent in the measurements. Given that observed nutrients are non-limiting, this suggests that the key mechanism relates to establishment of top-down control of the phytoplankton population being delayed and potentially under-represented in the model. Another biophysical mechanism apparent in the results is, while the model effectively simulates the accumulation of DIN forms in bottom waters through benthic connectivity and their subsequent lateral advection, the timing of the injection of these chemical constituents into surface waters is controlled by vertical mixing (i.e., reduction of vertical stratification). Thus, it is likely that the mismatch in surface nitrate and ammonium in the late fall, where the model values are too elevated, link back to stratification shortcomings noted above.

The principal motivation of developing a mechanistic dissolved oxygen formulation applicable to an estuarine system subject to significant riverine loadings and benthic connectivity has been realized with some success. The seasonal establishment of hypoxic bottom waters over the mid- to upper Bay, and the subsequent re-oxygenation in the fall, is well represented. Further, full anoxia in late summer in the upper Bay is also realized. An interesting result appearing in the model DO field is an association between hypoxia “hot spots” in the Bay and the inflows of the Patapsco and Choptank rivers. While they may primarily relate to estuarine circulation issues in the model, it is possible that these hot spots are indicative of the flow of low DO waters into the Bay from these riverine sources, and/or augmentation of the organic matter loads remineralized within the water column and by the benthos of the main stem Bay. While the impact of the multi-decadal trend in the Susquehanna’s nitrate loading on Bay eutrophication is well-established (Hagy et al. 2004), this model result suggests that the influence of the lower volume lateral riverine inputs to the main stem Bay play a significant role

in the establishment and maintenance of its hypoxic waters. Elucidating the effects of these lateral inputs deserves further investigation and assessment. This is particularly crucial in light of the amplifying anthropogenic impacts, associated with evolving land use and agricultural practices (among others), that are known to afflict river dominated estuarine and coastal waters worldwide (Zhang et al. 2010).

Two aspects of our model's biogeochemical function, both relating to how the transition from normoxic to anoxic remineralization is formulated, have demonstrated sensitivity that has clear repercussions on ecosystem behavior. These are: (1) introduction of asymmetry in the nitrification/denitrification ramps applied to the water column remineralization; and (2) modification of the half-saturation coefficient applied in linking benthic exchanges of DO and DIN to the dissolved oxygen concentration of overlying bottom waters. For the ramps asymmetry, the complexity of nitrogen cycling when a nitrification—denitrification coupling can be established at the boundary of oxygen deficient waters (Codispoti and Christensen 1985) strongly suggests that mirrored onset/shutdown of these processes in the water column is improbable and requires further consideration. The formulation we have introduced to link benthic remineralization with overlying dissolved oxygen concentration was developed with the objective to forego incorporating further complexity via coupling with a detailed benthic model (e.g., Soetaert et al. 2000). However, a very limited dataset was leveraged in developing our formulation; given the clear sensitivity to adjustment of its half-saturation parameter demonstrated by the model, a larger dataset that more comprehensively establishes these exchanges is desirable.

The sensitivity studies that we have documented clearly demonstrate that modification of the biogeochemical formulation leads to notable changes in the model's biological and chemical constituents. That is, biogeochemical controls on the Chesapeake Bay system, in particular the spatio-temporal distribution of its hypoxic waters, are of primary importance to attaining realistic biogeochemical function and, in this regard, are arguably on par with the influence of physical controls that has been elegantly demonstrated previously (Scully 2010, 2013). Consequently, a well-considered, mechanism-based biogeochemical model embedded within a coupled three-dimensional model framework is essential for achieving: (1) valuable insight into how short-term and interannual variation in river inflow and nutrient loading will impact the Chesapeake Bay estuarine system; (2) successful application of ecological prediction systems to promote informed recreational and resource use; and (3) accurate prediction of the biogeochemical and ecological consequences of climate change.

**Acknowledgements** The authors thank Wen Long, Jiangtao Xu, and Lyon Lanerolle for their contributions to the development of the ChesROMS biogeochemical model. We would also like to thank the two reviewers of our chapter for their insightful comments, which were extremely useful in improving this contribution. Funding for this work was primarily provided by the NOAA Center for Sponsored Coastal Ocean Research's Monitoring for Event Response for Harmful Algal Bloom (MERHAB) Program (NA05NOS4781222, NA05NOS4781226, NA05NOS4781227, and NA05NOS4781229). Additional support was provided by the NOAA EcoForecasting Program, the NOAA Center for Satellite Applications and Research, and Maryland Sea Grant. This is

MERHAB publication 189 and UMCES contribution no. 5138. The views, opinions, and findings contained in this report are those of the authors and should not be construed as an official NOAA or U.S. Government position, policy, or decision.

## References

- Bradley PB, Lomas MW, Bronk DA (2010) Inorganic and organic nitrogen use by phytoplankton along Chesapeake Bay, measured using a flow cytometric sorting approach. *Estuaries Coasts* 33(4):971–984. doi:[10.1007/s12237-009-9252-y](https://doi.org/10.1007/s12237-009-9252-y)
- Brown CW, Hood RR, Long W, Jacobs J, Ramers DL, Wazniak C, Wiggert JD, Wood R, Xu J (2013) Ecological forecasting in Chesapeake Bay: using a mechanistic-empirical modeling approach. *J Mar Syst* 113–125. doi:[10.1016/j.jmarsys.2012.12.007](https://doi.org/10.1016/j.jmarsys.2012.12.007)
- Codispoti LA, Christensen JP (1985) Nitrification, denitrification and nitrous oxide cycling in the Eastern Tropical South Pacific Ocean. *Mar Chem* 16:277–300
- Costantini M, Ludsin SA, Mason DM, Zhang X, Boicourt WC, Brandt SB (2008) Effect of hypoxia on habitat quality of striped bass (*Morone saxatilis*) in Chesapeake Bay. *Can J Fish Aquat Sci* 65(5):989–1002. doi:[10.1139/f08-021](https://doi.org/10.1139/f08-021)
- Cowan JLW, Boynton WR (1996) Sediment-water oxygen and nutrient exchanges along the longitudinal axis of Chesapeake Bay: seasonal patterns, controlling factors and ecological significance. *Estuaries* 19(3):562–580
- Decker MB, Brown CW, Hood RR, Purcell JE, Gross TF, Matanoski JC, Bannon RO, Setzler-Hamilton EM (2007) Predicting the distribution of the scyphomedusa *Chrysaora quinquecirrha* in Chesapeake Bay. *Mar Ecol Prog Ser* 329:99–113. doi:[10.3354/meps329099](https://doi.org/10.3354/meps329099)
- Feng Y, Friedrichs MAM, Wilkin J, Tian HQ, Yang QC, Hofmann EE, Wiggert JD, Hood RR (2015) Chesapeake Bay nitrogen fluxes derived from a land-estuarine ocean biogeochemical modeling system: model description, evaluation, and nitrogen budgets. *J Geophys Res* 120(8):1666–1695. doi:[10.1002/2015jg002931](https://doi.org/10.1002/2015jg002931)
- Fennel K, Wilkin J, Levin J, Moisan J, O'Reilly J, Haidvogel D (2006) Nitrogen cycling in the Middle Atlantic Bight: results from a three-dimensional model and implications for the North Atlantic nitrogen budget. *Global Biogeochem Cycles* 20(3). doi:[10.1029/2005GB002456](https://doi.org/10.1029/2005GB002456)
- Geider RJ, MacIntyre HL, Kana TM (1997) Dynamic model of phytoplankton growth and acclimation: Responses of the balanced growth rate and the chlorophyll a: carbon ratio to light, nutrient-limitation and temperature. *Mar Ecol Prog Ser* 148(1–3):187–200
- Goodrich DM, Blumberg AF (1991) The fortnightly mean circulation of Chesapeake Bay. *Estuar Coast Shelf Sci* 32(5):451–462
- Guo XY, Valle-Levinson A (2007) Tidal effects on estuarine circulation and outflow plume in the Chesapeake Bay. *Cont Shelf Res* 27(1):20–42. doi:[10.1016/j.csr.2006.08.009](https://doi.org/10.1016/j.csr.2006.08.009)
- Hagy JD, Boynton WR, Jasinski DA (2005) Modelling phytoplankton deposition to Chesapeake Bay sediments during winter-spring: interannual variability in relation to river flow. *Estuar Coast Shelf Sci* 62(1–2):25–40
- Hagy JD, Boynton WR, Keefe CW, Wood KV (2004) Hypoxia in Chesapeake Bay, 1950–2001: long-term change in relation to nutrient loading and river flow. *Estuaries* 27(4):634–658
- Huntley ME, Lopez MDG (1992) Temperature-dependent production of marine copepods: a global synthesis. *Am Nat* 140(2):201–242
- Jacobs JM, Rhodes M, Brown CW, Hood RR, Leight A, Long W, Wood R (2014) Modeling and forecasting the distribution of *Vibrio vulnificus* in Chesapeake Bay. *J Appl Microbiol* 117(5):1312–1327. doi:[10.1111/jam.12624](https://doi.org/10.1111/jam.12624)
- Kemp WM, Boynton WR, Adolf JE, Boesch DF, Boicourt WC, Brush G, Cornwell JC, Fisher TR, Glibert PM, Hagy JD, Harding LW, Houde ED, Kimmel DG, Miller WD, Newell RIE, Roman MR, Smith EM, Stevenson JC (2005) Eutrophication of Chesapeake Bay: historical trends and ecological interactions. *Mar Ecol Prog Ser* 303:1–29

- Kemp WM, Testa JM, Conley DJ, Gilbert D, Hagy JD (2009) Temporal responses of coastal hypoxia to nutrient loading and physical controls. *Biogeosciences* 6(12):2985–3008
- Ludsin SA, Zhang X, Brandt SB, Roman MR, Boicourt WC, Mason DM, Costantini M (2009) Hypoxia-avoidance by planktivorous fish in Chesapeake Bay: implications for food web interactions and fish recruitment. *J Exp Mar Biol Ecol* 381:S121–S131. doi:[10.1016/j.jembe.2009.07.016](https://doi.org/10.1016/j.jembe.2009.07.016)
- Meyers T, Sickles J, Dennis R, Russell K, Galloway J, Church T (2001) Atmospheric nitrogen deposition to coastal estuaries and their watersheds. In: Valigura RA, Alexander RB, Castro MS, Meyers TP, Paerl HW, Stacey PE, Turner RE (eds) Nitrogen loading in coastal water bodies: an atmospheric perspective. American Geophysical Union, Washington D. C., p 254
- Middelburg JJ, Soetaert K, Herman PMJ, Heip CHR (1996) Denitrification in marine sediments: a model study. *Global Biogeochem Cycles* 10(4):661–673
- Moore KA, Jarvis JC (2008) Environmental factors affecting recent summertime eelgrass diebacks in the lower Chesapeake Bay: implications for long-term persistence. *J Coast Res* 135–147. doi:[10.2112/si55-014](https://doi.org/10.2112/si55-014)
- Moore KA, Wetzel RL (2000) Seasonal variations in eelgrass (*Zostera marina* L.) responses to nutrient enrichment and reduced light availability in experimental ecosystems. *J Exp Mar Biol Ecol* 244(1):1–28. doi:[10.1016/s0022-0981\(99\)00135-5](https://doi.org/10.1016/s0022-0981(99)00135-5)
- Murphy R, Kemp W, Ball W (2011) Long-term trends in Chesapeake Bay seasonal hypoxia, stratification, and nutrient loading. *Estuaries Coasts* 34(6):1293–1309. doi:[10.1007/s12237-011-9413-7](https://doi.org/10.1007/s12237-011-9413-7)
- Najjar RG, Pyke CR, Adams MB, Breitburg D, Hershner C, Kemp M, Howarth R, Mulholland MR, Paolisso M, Secor D, Sellner K, Wardrop D, Wood R (2010) Potential climate-change impacts on the Chesapeake Bay. *Estuar Coast Shelf Sci* 86(1):1–20
- National Marine Fisheries Service (2011) Fisheries economics of the United States, 2009. Economics and sociocultural status and trends series. U.S. Department of Commerce, Silver Spring, MD
- Oguz T (2002) Role of physical processes controlling oxycline and suboxic layer structures in the Black Sea. *Global Biogeochem Cycles* 16(2). doi:[10.1029/2001GB001465](https://doi.org/10.1029/2001GB001465)
- Pace ML, Carpenter SR, Cole JJ (2015) With and without warning: managing ecosystems in a changing world. *Front Ecol Environ* 13(9):460–467. doi:[10.1890/150003](https://doi.org/10.1890/150003)
- Rabalais NN, Diaz RJ, Levin LA, Turner RE, Gilbert D, Zhang J (2010) Dynamics and distribution of natural and human-caused hypoxia. *Biogeosciences* 7(2):585–619
- Rysgaard S, Risgaard-Petersen N, Sloth NP, Jensen K, Nielsen LP (1994) Oxygen regulation of nitrification and denitrification in sediments. *Limnol Oceanogr* 39(7):1643–1652
- Sanford LP, Suttles SE, Halka JP (2001) Reconsidering the physics of the Chesapeake Bay estuarine turbidity maximum. *Estuaries* 24(5):655–669
- Schubel J, Pritchard D (1986) Responses of upper Chesapeake Bay to variations in discharge of the Susquehanna River. *Estuaries Coasts* 9(4):236–249
- Scully ME (2010) Wind modulation of dissolved oxygen in Chesapeake Bay. *Estuaries Coasts* 33(5):1164–1175. doi:[10.1007/s12237-010-9319-9](https://doi.org/10.1007/s12237-010-9319-9)
- Scully ME (2013) Physical controls on hypoxia in Chesapeake Bay: a numerical modeling study. *J Geophys Res* 118(3):1239–1256. doi:[10.1002/jgrc.20138](https://doi.org/10.1002/jgrc.20138)
- Shchepetkin AF, McWilliams JC (2005) The regional oceanic modeling system (ROMS): a split-explicit, free-surface, topography-following-coordinate oceanic model. *Ocean Model* 9(4):347–404
- Soetaert K, Middelburg JJ, Herman PMJ, Buis K (2000) On the coupling of benthic and pelagic biogeochemical models. *Earth Sci Rev* 51(1–4):173–201
- Willmott CJ (1981) On the validation of models. *Phys Geogr* 2(2):184–194. doi:[10.1080/02723646.1981.10642213](https://doi.org/10.1080/02723646.1981.10642213)
- Xu J, Long W, Wiggert JD, Lannerolle LWJ, Brown CW, Murtugudde R, Hood RR (2011) Climate forcing and salinity variability in the Chesapeake Bay, USA. *Estuaries Coasts*. doi:[10.1007/s12237-011-9423-5](https://doi.org/10.1007/s12237-011-9423-5)

- Xu JT, Hood RR, Chao SY (2005) A simple empirical optical model for simulating light attenuation variability in a partially mixed estuary. *Estuaries* 28(4):572–580
- Zhang J, Gilbert D, Gooday AJ, Levin L, Naqvi SWA, Middelburg JJ, Scranton M, Ekau W, Pena A, Dewitte B, Oguz T, Monteiro PMS, Urban E, Rabalais NN, Ittekkot V, Kemp WM, Ulloa O, Elmgren R, Escobar-Briones E, Van der Plas AK (2010) Natural and human-induced hypoxia and consequences for coastal areas: synthesis and future development. *Biogeosciences* 7(5):1443–1467. doi:[10.5194/bg-7-1443-2010](https://doi.org/10.5194/bg-7-1443-2010)